Appl. Phys. B (2017) 123:136
DOI 10.1007/s00340-017-6705-z

Applied Physics B
Lasers and Optics

Characterization of strongly scattering nanoporous materials as miniaturized multipass cell for tunable diode laser absorption spectroscopy

F. Venturini[1] · V. Schönherr[1] · J. M. Rey[1] · E. Adolfsson[2]

Received: 6 January 2017 / Accepted: 20 March 2017 / Published online: 10 April 2017
© Springer-Verlag Berlin Heidelberg 2017

Abstract Through the confinement of gas in nanoporous materials, it is possible to significantly increase the path length for light–gas interaction. This enables the observation of much stronger absorption features for the confined gas molecules. In this work, we systematically characterized a variety of disordered strongly scattering ZrO_2 and Al_2O_3 nanoporous ceramic materials to exploit the potential of gas in scattering media absorption spectroscopy. As a result, we identified a material with an unprecedented performance in terms of optical path length enhancement. In ZrO_2 with thicknesses above 6 mm, the path enhancement exceeds 1000. The results obtained with near-infrared absorption spectroscopy on oxygen were validated by time-of-flight measurements at 700 nm, thus demonstrating their robustness. Finally, we report quantitative oxygen concentration measurement using nanoporous materials as miniaturized random-scattering multipass cell with an extremely simple and low-cost setup.

This article is part of the topical collection "Field Laser Applications in Industry and Research" guest edited by Francesco D'Amato, Erik Kerstel, and Alan Fried.

✉ F. Venturini
francesca.venturini@zhaw.ch

[1] Institute of Applied Mathematics and Physics, Zurich University of Applied Sciences, Technikumstrasse 9, 8401 Winterthur, Switzerland

[2] Ceramic Materials, SWEREA IVF, Box 104, 431 22 Mölndal, Sweden

1 Introduction

Tunable diode laser absorption spectroscopy (TDLAS) is a well-established technique for selective gas sensing both in research and industrial fields. Efforts towards improving detection limits have pushed the research for long light–sample interaction path lengths. Some of the most widespread strategies include, for example, the use of conventional multipass gas cells (White [1], Herriott [2] and Pfund cells [3]), and circular optical cells [4]. These sample cells usually allow reaching long path lengths but have a complex setup and alignment. Furthermore, particularly in industrial and medical fields, there is the necessity to minimize the sampled volume for the gas measurement. To solve these issues, several approaches have been studied in the last years, as the inclusion of transmissive or reflective optical diffusers [5], filled integrating spheres [6] and gas filled hollow core fibers [7, 8]. A relatively new approach to achieve both long interaction path lengths, minimal sample gas volume, and extremely easy alignment is to use porous media to increase the light–gas interaction through strong scattering. This approach, also known as gas in scattering media absorption spectroscopy (GASMAS) [9], allows to use the porous material as a miniaturized random-scattering multipass cell [10–14]. Mean optical path length (MOPL) enhancements up to 750 were reported in ZrO_2 [11]. In this work, we investigate, in detail, the influence of the material properties and preparation method on the scattering of light and on the MOPL in the samples to further push the MOPL enhancement and explore the limits of this approach.

To investigate the propagation of light in the nanoporous ceramics, we used two measuring techniques: near-infrared TDLAS on confined oxygen molecules and photon time-of-flight (TOF) spectroscopy. We then compared the MOPL

of the diffused light obtained with the two methods and demonstrated the robustness of the results. The nanoporous materials studied are Al_2O_3 and ZrO_2, with focus on ZrO_2 because of the strongest enhancement of the MOPL.

By a systematic investigation of a large number of samples, we were able to identify a material which, to the best of our knowledge, enables an unprecedented MOPL enhancement. Using direct absorption spectroscopy and a minimal setup, we demonstrate that this material can be used as miniaturized random-scattering multipass cell for oxygen detection by TDLAS.

2 Material preparation and characterization

To analyze the influence of the structure and of the porosity on the optical properties, several samples were prepared using different starting material and preparation methods. An overview of the samples studied and of their properties is shown in Table 1. All nanoporous materials were prepared starting from commercially available powders: Al_2O_3 samples were prepared using α-alumina single crystal with 0.4 µm grain size from Sumitomo, Japan; ZrO_2 samples were prepared using zirconia powders with 40 and 90 nm grain size from Tosoh, Japan. The pore size and porosity, defined as ratio of the total pore volume to the total sample volume [15], were measured by mercury intrusion (Auto Pore III 9410, Micromeritics).

All samples prepared by compaction of granules were uniaxially pre-pressed at a low pressure in a steel die followed by cold isostatic pressing (CIP) at pressures between 50 and 300 MPa, and then were sintered in air at 900 °C for 2 h. The samples of the type Z8–Z11 were prepared by heat treatment of the powder at different temperatures between 600 and 1200 °C to increase the crystallinity and modify the particles before compaction. The heat-treated powders were ball milled using zirconia milling media to remove agglomerates. An addition of 3 wt% of polyethylene glycol (PEG) was added as binder followed by freeze granulation and freeze drying of the prepared granules. Samples from these modified zirconia materials were finally prepared by compaction and sintering using the same procedure as for the non heat-treated powders.

The changes in the morphology due to the different material and preparation methods are clearly visible in scanning electron microscope images, as shown in Fig. 1, for selected materials. The material of the type Z1 (Fig. 1a) has the smallest pore size (42 nm). The materials of the types Z5 and Z7 differ only on the compaction pressure which results in a slightly larger size of the pores, visible from the picture (Fig. 1b, d). The material Z9, which was heat treated at 900 °C before compaction, is characterized by larger grains which agglomerate and result in lower pore size (73 nm) (Fig. 1c).

3 Experiment

The setup for the absorption spectroscopy experiments is shown schematically in Fig. 2. The light source is a 0.25 mW single-mode VCSEL (760nm TO5 VCSEL, Philips Photonics) emitting at 760 nm. The laser current and temperature were adjusted by a temperature controller (TEC 2000, Thorlabs) and a VCSEL laser diode controller (LDC 200C, Thorlabs). The light transmitted by the sample is collected using a large-area Si $10 \times 10\,mm^2$ photodiode (FS1010, Thorlabs) and amplified by an adjustable-gain photodiode amplifier (PDA200C, Thorlabs). The current

Table 1 Overview of the material studied

Material	Powder	Preparation	Median pore diameter (nm)	Porosity (%)	Identifier
Al_2O_3	aa04	Slipcast	142	47	A1
ZrO_2	TZ3YBE	CIP 300 MPa	42	49	Z1
ZrO_2	TZ3YSE	Slipcast	119	49	Z2
ZrO_2	TZ3YSE	CIP 300 MPa, granulated	75	47	Z3
ZrO_2	TZ-0	CIP 300 MPa	47	47	Z4
ZrO_2	TZ3YSBE	CIP 300 MPa	98	49	Z5
ZrO_2	TZ3YSBE	CIP 100 MPa	120	53	Z6
ZrO_2	TZ3YSBE	CIP 50 MPa	130	55	Z7
ZrO_2	TZ3YSBE	ht* 600 °C, g**, CIP 300 MPa	89	48	Z8
ZrO_2	TZ3YSBE	ht* 900 °C, g**, CIP 300 MPa	73	46	Z9
ZrO_2	TZ3YSBE	ht* 1100 °C, g**, CIP 300 MPa	121	47	Z10
ZrO_2	TZ3YSBE	ht* 1200 °C, g**, CIP 300 MPa	85	47	Z11

* ht the powder was heat-treated at the indicated temperature before granulation and compaction; **g granulated; CIP cold isostatic pressing at the indicated pressure

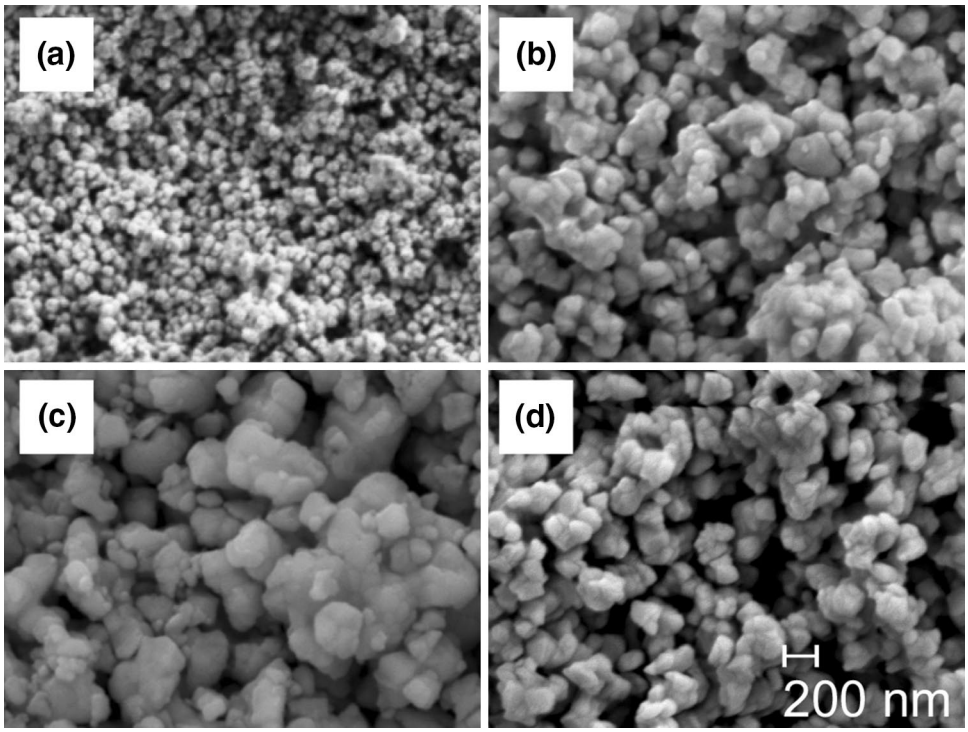

Fig. 1 Scanning electron microscope images of selected nanoporous material: **a** type Z1, **b** type Z5, **c** type Z9, and **d** sample of the type Z7

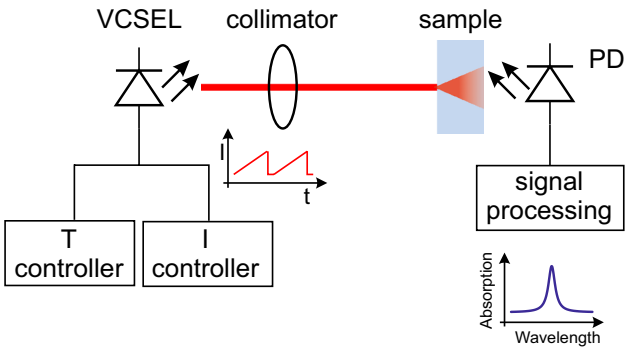

Fig. 2 Schematic diagram of the setup used for the absorption spectroscopy experiments. *PD* photodiode

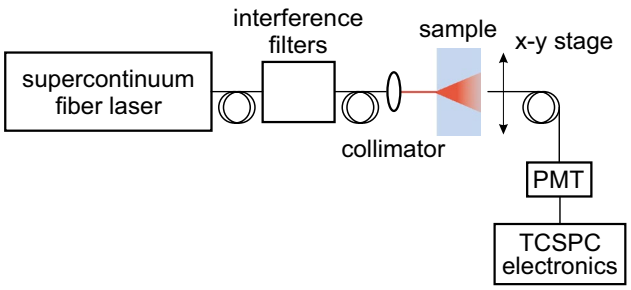

Fig. 3 Schematic diagram of the setup used for the TOF experiments. *PMT* photomultiplier, *TCSPC* time-correlated single-photon counting

ramp for the wavelength-sweep and the data acquisition were performed by a DAQ card (USB-6361, National Instrument) using a Labview^{TM} software. The laser current sweep was chosen so to be able to measure three oxygen absorption lines, as discussed in Sect. 4. The total distance between the laser and the detector was kept fixed at 10 cm. It is possible to reduce this dimension to the mechanical minimum of a few millimeters. We chose this distance to be able to perform a sufficiently robust reference measurement in air also without nanoporous sample. All the measurements reported here are performed in air, at room temperature and pressure ($T = 296$ K, $p = 1$ atm, 21% O_2).

Figure 3 shows the setup for the TOF experiments. The light source is a super-continuum fiber laser (SuperK Extreme, NKT Photonics) pulsed at 3.55 MHz. The light continuum was filtered by motorized interference filters (SuperK Varia, NKT Photonics). The excitation light was centred at 700 nm with a 10 nm FWHM and a 50 dB out-of-band suppression. Pulse durations at this wavelength were typically below 100 ps. Light was delivered by a fiber to the sample and collimated to a diameter of approximately 1 mm. The light transmitted by the sample was collected by a fiber and detected by a photomultiplier (PMA175, PicoQuant) and a time-correlated single-photon counting card (TimeHarp Pico, PicoQuant).

To characterize the light transmission through samples, a calibrated silicon detector (918D-SL-OD3, Newport) was used.

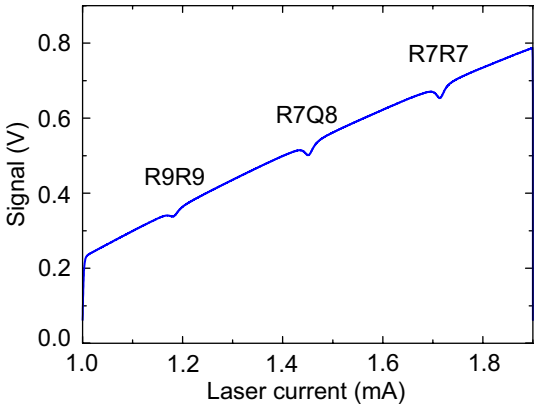

Fig. 4 Typical recorded raw signal for three oxygen lines R9R9 (760.77 nm), R7Q8 (760.89 nm), and R7R7 (761.003 nm) of the O_2 near-infrared A-band. The measurement is taken at atmospheric conditions with a sample of the type Z5 with a thickness of 4.8 mm. The signal is the average of 1000 single scan acquisitions

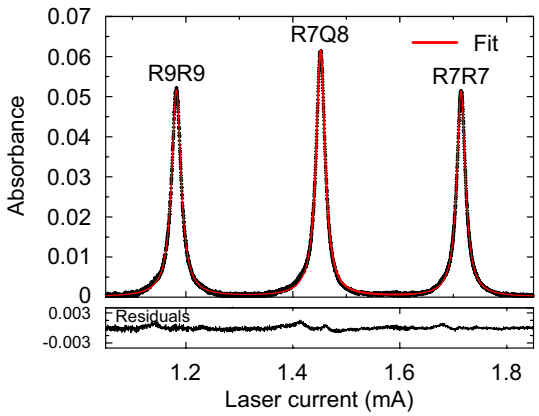

Fig. 5 Typical absorbance for the three oxygen lines R9R9 (760.77 nm), R7Q8 (760.89 nm), and R7R7 (761.003 nm) of the O_2 near-infrared A-band. The measurement is taken at atmospheric conditions with a sample of the type Z5 having a thickness of 4.8 mm. *Red solid line*: fit using a Lorentzian profile. The residuals are shown in the lower panel

4 Data analysis

The absorption MOPL of the gas confined in the samples was determined using the three strong lines R9R9 (760.77 nm), R7Q8 (760.89 nm), and R7R7 (761.00 nm) of the O_2 near-infrared A-band. A typical spectroscopic raw transmitted signal is shown in Fig. 4.

The large number of collisions against the nanoporous material results in a significant collisional broadening of the absorption lines compared to the free O_2. This broadening depends on the pore size and, therefore, on the material. For example, the broadening factor of the line R7Q8 ranges between 1.29, for samples of the type A1, to 1.59 for samples of the type Z1, consistent with previously reported values [11, 16]. Since the spectral tails of neighboring lines overlap due to this broadening, it is important to fit the measured signal in nanoporous material considering several lines at the same time. In this work, three lines were measured and simultaneously fitted by a function which is the sum of a polynomial of the fourth order, to account for the non-linear wavelength-dependent intensity of the laser, and three Lorentzian, one for each line to be fitted. The fit was performed using a non-linear squares routine.

The absorbance after the baseline subtraction is shown in Fig. 5 together with the best fit. For all the materials investigated in this work, the absorption lines can be fitted well by a Lorentzian profile. The very good agreement of the fit with the experimental data indicates that line broadening due to the wall collisions [11, 17] and pressure dominates over Doppler broadening at ambient conditions. The use of a Voigt profile would be necessary, however, at lower pressures or higher temperatures [18, 19].

The absorption path length in a nanoporous sample is an unknown quantity and depends strongly on the material properties. Being actually an average of many paths through the material, it is more properly referred to as mean absorption path length and will be indicated here as $L^{\text{gas}}_{\text{mean}}$. This quantity is defined as the distance the light would travel in air to experience the same fractional absorption as in the scattering medium [20]. $L^{\text{gas}}_{\text{mean}}$ can be determined as the ratio of the signal obtained at a reference measurement with a known absorption length. As reference, we chose a measurement in air at the same exact conditions. The mean absorption path length was, therefore, calculated as

$$L^{\text{gas}}_{\text{mean}} = L_0 \frac{A_{\text{sample}}}{A_0} \tag{1}$$

with L_0 the optical absorption path length in air, A_{sample} and A_0 the area of the absorption line with the sample and in air, respectively. The choice of the area instead of the peak maximum is motivated by the large material-dependent line broadening discussed previously.

To compare the results of the two measuring techniques, we have determined the MOPL L_{mean} in the material from the TOF measurements as [15, 20, 21]

$$L_{\text{mean}} = c \ < t > \tag{2}$$

where c is the speed of light in air and $< t >$ is the weighted average of the transmitted intensity distribution $T(t)$ and is given by

$$< t > = \frac{\int_0^\infty T(t)\, t \, \mathrm{d}t}{\int_0^\infty T(t) \, \mathrm{d}t}. \tag{3}$$

Light propagating in a nanoporous material will be passing both through the pores, filled with the gas, and through the matrix material, for example ZrO_2. The mean path length through the pores and through the matrix can be denoted as $L_{\text{mean}}^{\text{gas}}$ and $L_{\text{mean}}^{\text{solid}}$, respectively. The total MOPL in the material can be defined as [22, 23]

$$L_{\text{mean}} = L_{\text{mean}}^{\text{gas}} + L_{\text{mean}}^{\text{solid}}. \quad (4)$$

Absorption spectroscopy measurement leads to the determination of $L_{\text{mean}}^{\text{gas}}$. L_{mean} can then be calculated considering the porosity of the sample. For example, for a sample with a porosity of 50%, as most of the samples studied in this work, the physical path in the gas and that in the material of the matrix are the same. It follows that, writing $L_{\text{mean}}^{\text{solid}} = n\, L_{\text{mean}}^{\text{gas}}$, the MOPL L_{mean} can be calculated as

$$L_{\text{mean}} = (1 + n)\, L_{\text{mean}}^{\text{gas}} \quad (5)$$

with n being the refraction index of the material.

5 Results and discussion

To use these materials as miniature multipass cell, it is necessary to achieve the highest possible optical absorption path length. On the other hand, an increased MOPL is associated with an increased scattering. This negatively impacts on the signal obtained from the photodiode due to the increase in the solid angle of the transmitted light and to the consequently lower collected light intensity. Although a long path length is most desirable for TDLAS, the low transmitted intensity poses a challenge for the detection. For practical purposes, therefore, the choice of the optimal material should be a compromise between these two aspects.

The transmitted light power was first investigated to characterize the samples systematically. The inverse of the transmission for different materials as a function of the sample thickness is shown in Fig. 6. According to classical diffusion theory, the inverse of the transmission should depend linearly from the thickness of the sample [24–27]. The non-linear dependence shown in Fig. 6 can, however, be explained with the finite detection area of the power meter, as previously described [24]. As expected, this effect is more pronounced for materials which exhibit stronger scattering (type Z5 and Z7). Figure 6 also shows that ZrO_2 samples with smaller pores (type Z1, 42 nm) are characterized by a higher transmission than samples with larger pore sizes (types Z5 and Z7, 98 and 130 nm, respectively), indicating a weaker scattering. In addition, samples of Al_2O_3 (type A1) which have a median pore diameter of 142 nm are characterized by a low transmission comparable to that of the ZrO_2 type Z7 with a median pore diameter of 130 nm, indicating a similarly strong scattering.

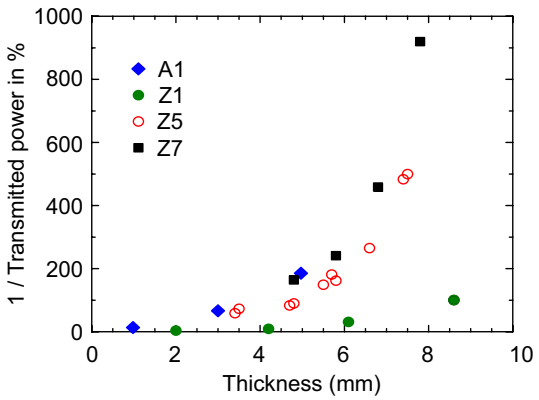

Fig. 6 Inverse of the power transmitted through a sample as a function of the sample thickness for different materials

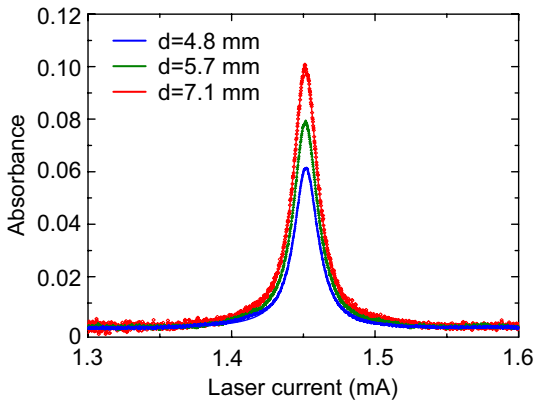

Fig. 7 Absorption signal of the R7Q8 oxygen line for different thicknesses d of samples of type Z5. Points are measurement; *solid lines* are Lorentzian fits

Using absorption spectroscopy with known oxygen concentration, it is possible to determine the MOPL in the gas $L_{\text{mean}}^{\text{gas}}$. Being the result of many different paths, the quantity $L_{\text{mean}}^{\text{gas}}$ depends on the illumination and detection geometry. It is not a fixed, material-dependent quantity but describes the average distance traveled in the gas.

Keeping the illumination and detection geometry identical for all the experiments, we investigated the dependence of the absorption line on the material and, for a given type, the effect of the sample thickness. A typical result is shown in Fig. 7 for samples of type Z5 of three thicknesses. As expected, increasing the thickness results in a stronger absorbance indicating a longer MOPL in gas. For the sample with the greater thickness the reduction of the transmitted intensity manifests itself as a noise increase (Fig. 7). This can be quantified by the signal-to-noise (S/N) ratio calculated as the ratio of the absorbance peak of the R7Q8 line and one σ of the background. In Fig. 7, the S/N ratio

is ca. 230 for the sample with $d = 4.8$ and $d = 5.7$ mm and decreases to ca. 120 for the sample with $d = 7.1$ mm.

The characterization of representative samples is summarized in Fig. 8, where the equivalent mean path length determined by absorption spectroscopy $L_{\text{mean}}^{\text{gas}}$ for the different materials is shown as a function of the thickness of the samples. For clarity, only the results of the types A1, Z1, Z5, and Z7 are shown. These materials display the most representative behaviors. The longest MOPL in gas was obtained with samples of the type Z7, which are characterized by the highest porosity. Similar material (Z5) with lower porosity has a much shorter effective gas–light interaction path. Samples of the type A1, although having slightly lower porosity than of the type Z1, perform significantly better, showing that the pore size together with the porosity plays an important role.

The samples of the type Z2 and Z3 exhibit a $L_{\text{mean}}^{\text{gas}}$ between the values measured for Z1 and Z5. Z4 type samples perform similarly to those of the type Z1, samples of type Z6 to type Z7, with a slightly lower $L_{\text{mean}}^{\text{gas}}$. Finally, the samples Z8–Z11 perform poorly due an extremely low transmitted power.

As expected from classical diffusion theory [25], $L_{\text{mean}}^{\text{gas}}$ depends quadratically on the thickness of the material (Fig. 8). This is consistent with the previous results on polystyrene foams [15], macroporous gallium phosphide [26] and pharmaceutical tablets of microcrystalline cellulose [20].

The effect of the thickness on the increase of the MOPL can be best evidenced by plotting the path enhancement in the material as a function of the sample thickness. The path enhancement is defined as the ratio of $L_{\text{mean}}^{\text{gas}}$ and the sample thickness, and is a measure of how much the mean optical path length in the gas is being increased due to strong scattering. As visible in Fig. 9, the path enhancement increases linearly with the thickness of the sample for all the materials studied in this work. For the material of type Z7, it was possible to measure an enhancement of above 1000 times, which is higher than previously reported values [11]. This enormous increase is stronger than the increased noise due to the reduced transmitted intensity and results in a S/N of ca. 290 for sample thicknesses of $d = 7.5$ mm. This leads to a rough estimate of the resolution of ca. 0.7‰ O_2. For comparison, the same geometry without a nanoporous material would allow with our setup a resolution of ca. 3% O_2.

To validate the results obtained with absorption spectroscopy, the MOPL was also determined by time-of-flight measurements. The effect of increasing thickness for a single type of samples (Z5) is shown in Fig. 10. With increasing thickness, the average transit time $< t >$

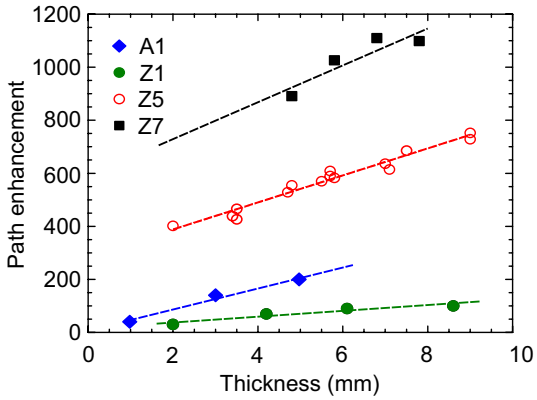

Fig. 9 Absorption path enhancement from oxygen measurements as a function of the sample thickness for different materials. The *dashed lines* are a linear fit

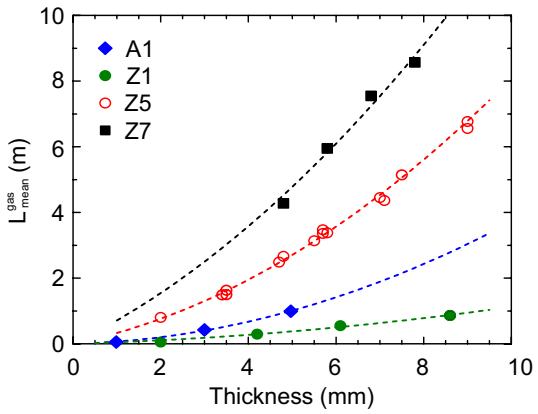

Fig. 8 Equivalent mean path length in gas from oxygen measurements as a function of the sample thickness for various materials. The *dashed lines* are second-order polynomial function

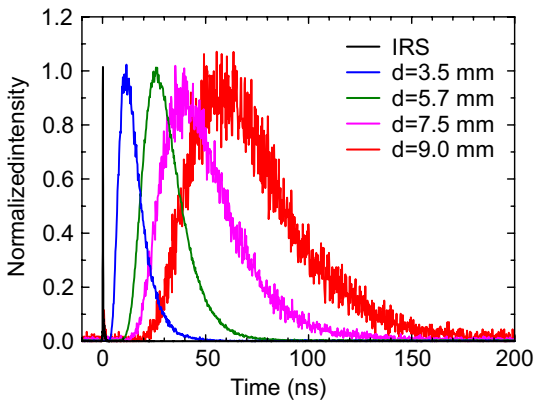

Fig. 10 Transmitted light intensity distribution through samples of the type Z5 with increasing thicknesses. *IRF* instrument response function

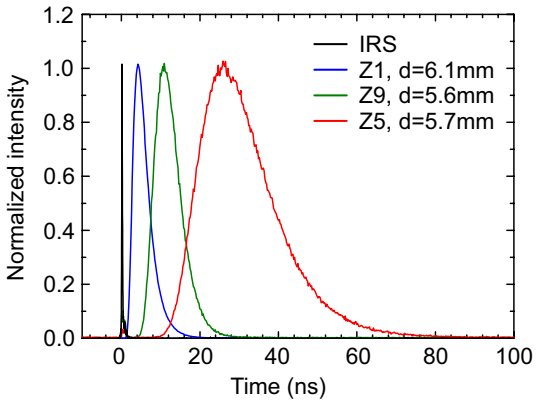

Fig. 11 Transmitted light intensity distribution through different type of samples. *IRF* instrument response function

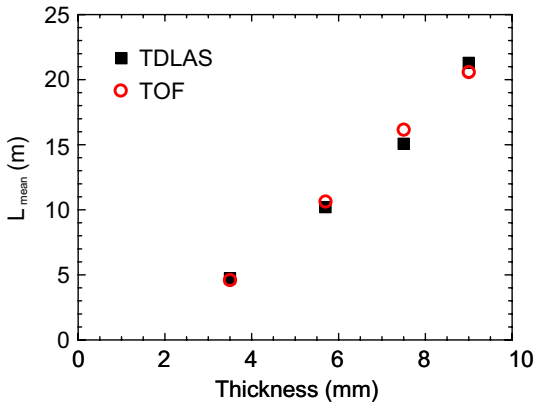

Fig. 12 Comparison of the MOPL L_{mean} for samples of the type Z5 for different thicknesses. *Black squares* results determined from absorption spectroscopy measurements (TDLAS), *red circles* results from TOF measurements (TOF)

, calculated as described in Sect. 4, becomes longer due to the increased scattering. The noise also becomes evidently much higher as a direct consequence of the reduced transmitted intensity (as shown in Fig. 6).

The transmitted light intensity distribution for selected samples materials of approximately the same thickness is shown in Fig. 11. Consistently with the gas absorption results, samples of the type Z1 display lower scattering than type Z9 and Z5. In Figs. 10 and 11, the incident light pulse is also visible as a narrow peak centred around the time origin. Since this peak, which represents the instrument response function (IRF) is shorter than 100 ps, there was no need to perform a deconvolution between the measured intensities and the IRF.

The MOPL L_{mean} calculated as described in Sect. 4 with the two experimental methods as a function of the thickness for Z5 type samples is shown in Fig. 12. This figure shows that there is a very good agreement between the results obtained with the two methods, thus demonstrating the robustness of the experimentally determined MOPL values. The small discrepancies observed can be due to the error on the porosity value and to the slight differences in the illumination and detection geometries. Moreover, the TDLAS signal results from a spacial average and the TOF one from a time average on a small spacial area.

6 Conclusions

In this work, we analyzed a large number of nanoporous materials, particularly of ZrO_2, to characterize their properties and determine the material most suited to be used as miniaturized random-scattering multipass gas cell. Compared to the previous works exploiting this method, we realized an extremely simple and low-cost setup, with no moving parts, like dithering coils, that performs well using simple direct absorption spectroscopy. This choice was motivated by the interest to demonstrate that this technique can be used for a commercial sensing solution. Particularly in industrial applications costs, minimal sample gas volumes, ease of alignment, and operation are major requirements.

The analysis covered a large number of samples obtained with different materials and preparation methods. By comparing the MOPL obtained with two independent methods, TDLAS and TOF spectroscopy, we were able to demonstrate the robustness of the results. The best material among those studied is the type Z7 (ZrO_2, with mean pore diameter of 130 nm and 56% porosity). For Z7 nanoporous samples with thickness above 6 mm, the path enhancement exceeds 1000.

From our analysis, it also emerged that both porosity and pore size determine the scattering of light in the material: higher porosity leads to stronger scattering and, therefore, larger MOPLs; for similar porosity, the samples with larger pore size showed stronger path length enhancement.

An important aspect to consider for practical applications is the adsorption of gases by the inner surface of the nanoporous material. It is expected that changes in the surface refractive index would affect the scattering and, therefore, the resulting MOPL. Therefore, the most appropriate material must be chosen depending on the sensing application. A further aspect for a sensor system is the response time to gas changes. This is determined by the diffusion of the gas into the material, and, therefore, depends on both the diffusing gas and the material properties like porosity and thickness. Since oxygen diffusion in nanoporous material is a rapid process [28], the response time is expected to be reasonably fast.

In conclusion, this work shows that nanoporous material like ZrO_2 with porosity above 50% can be used as multipass

gas cell of extremely reduced dimensions and with a very simple setup for quantitative oxygen measurement.

This work was carried out under a Commission for Technology and Innovation CTI Grant (17176.1 PFNM-NM). The authors would like to thank Yoram de Hazan of the Institute of Applied Mathematics and Physics, Zurich University of Applied Sciences, Switzerland, for the SEM images of the samples and Sven Karlsson of SWEREA IVF, Sweden, for the porosity measurement of the samples.

References

1. J.U. White, J. Opt. Soc. Am. **32**, 285–288 (1942)
2. D.R. Herriott, H.J. Schulte, Appl. Opt. **4**, 883–889 (1965)
3. W.S. Dalton, H. Sakai, Appl. Opt. **19**, 2413–2415 (1980)
4. A. Manninen, B. Tuzson, H. Looser, Y. Bonetti, L. Emmenegger, Appl. Phys. B **109**, 461–466 (2012)
5. J. Hodgkinson, D. Masiyano, R.P. Tatam, Appl. Phys. B **100**, 291–302 (2010)
6. D. Masiyano, J. Hodgkinson, R.P. Tatam, Appl. Phys. B **100**, 303–12 (2010)
7. J. Chen, A. Hangauer, R. Strzoda, M.C. Amann, Appl. Opt. **49**(28), 5254–5261 (2010)
8. G. Fetzer, A. Pittner, W. Ryder, D. Brown, Appl. Opt. **41**, 3613–3621 (2002)
9. M. Sjholm, G. Somesfalean, J. Alnis, S. Andersson-Engels, S. Svanberg, Opt. Lett. **26**, 16–18 (2001)
10. Y.N. Ponomarev, T.M. Petrova, A.M. Solodov, A.A. Solodov, Opt. Express **18**(25), 26062 (2010)
11. T. Svensson, E. Adolfsson, M. Lewander, C.T. Xu, S. Svanberg, Phys. Rev. Lett. **107**, 143901 (2011)
12. J.V. Auwera, N.H. Ngo, H. El Hamzaoui, B. Capoen, M. Bouazaoui, P. Ausset, C. Boulet, J.-M. Hartmann, Phys. Rev. Lett. A **88**, 042506 (2013)
13. Y. Ding, H. Lin, C. Yan, in Asia Communications and Photonics Conference 2014, OSA Technical Digest (online), paper ATh3A.190 (2014)
14. L. Yang, G. Somesfalean, S. He, Opt. Express **22**(3), 2584 (2014)
15. G. Somesfalean, M. Sjholm, J. Alnis, C. af Klinteberg, S. Andersson-Engels, S. Svanberg, Appl. Opt. **41**(18), 3538–3544 (2002)
16. T. Svensson, Z. Shen, Appl. Phys. Lett. **96**, 021107 (2010)
17. M. Danos, S. Geschwind, Phys. Rev. **91**(5), 1159–1162 (1953)
18. J.-M. Hartmann, V. Sironneau, T. Svensson, J.T. Hodges, C.T. Xu, Phys. Rev. A **87**, 032510 (2013)
19. C.T. Xu, M. Lewander, S. Andersson-Engels, E. Adolfsson, T. Svensson, S. Svanberg, Phys. Rev. A **84**, 042705 (2011)
20. T. Svensson, M. Andersson, L. Rippe, S. Svanberg, S. Andersson-Engels, J. Johansson, S. Folestad, Appl. Phys. B **90**, 345–354 (2008)
21. L. Mei, P. Lundin, S. Andersson-Engels, S. Svanberg, G. Somesfalean, Appl. Phys. B **109**, 467–475 (2012)
22. L. Mei, G. Somesfalean, S. Svanberg, Appl. Phys. A **114**, 393–400 (2014)
23. T. Svensson, E. Alerstam, E. Johansson, S. Andersson-Engels, Opt. Lett. **35**(11), 1740–1742 (2010)
24. I.M. Vellekoop, P. Lodahl, A. Lagendijk, Phys. Rev. E **71**, 056604 (2005)
25. D.J. Durian, Phys. Rev. E **50**(2), 857–866 (1994)
26. P.M. Johnson, A. Imhof, B.P.J. Bret, J.G. Rivas, A. Lagendijk, Phys. Rev. E **68**, 016604 (2003)
27. M.C.W. van Rossum, T.M. Nieuwenhuizen, Rev. Mod. Phys. **71**(1), 313–371 (1999)
28. T. Svensson, M. Lewander, S. Svanberg, Opt. Express **18**, 16460 (2010)